Subadditive femtosecond laser-induced electron emission from a GaAs tip

William Newman,[*] Eric R. Jones,[†] Evan Brunkow,[‡] Herman Batelaan,[§] and T. J. Gay[‖]
Jorgensen Hall, University of Nebraska, Lincoln, Nebraska 68588, USA

(Received 28 July 2023; revised 28 January 2024; accepted 2 April 2024; published 1 May 2024)

Multiphoton emission of electrons has been observed from sharp tips of heavily *p*-doped GaAs caused by laser pulses with, nominally, 800-nm wavelength, 1-nJ/pulse energy, and 90-fs duration. The emission is mostly due to four-photon processes, with some contribution from three-photon absorption as well. When the electron emission current due to two pulses separated by delay 200 fs $\leqslant \tau \leqslant$ 1 ns is integrated over all electron energies, it is less than that observed for the sum of the emission from the two individual pulses. This subadditive behavior is consistent with a fast electron emission process, i.e., one in which the electron emission occurs over a time comparable to the laser pulse width. The subadditivity results from Pauli blocking of electron emission by the second pulse due to a population increase of the GaAs conduction band caused by the first pulse. Such subadditive photoemission is a sensitive probe of excited-carrier dynamics. We employ the use of an excited-level population model to characterize the photon absorption process and give us a clearer understanding of the electron dynamics in GaAs associated with multiphoton electron emission. Possible applications of this subadditivity effect to control photoemitted electron spin are discussed.

DOI: 10.1103/PhysRevB.109.184101

I. INTRODUCTION

Gallium arsenide (GaAs) photoemitters have been studied extensively due, in part, to their ability to produce polarized electrons when optically pumped by continuous wave (CW) circularly polarized light of nominal wavelength 800 nm [1,2]. This wavelength causes direct band-gap transitions near the Γ point. Because of the relative excitation transition probabilities for the upper-level spin states when circularly polarized light is used, the electrons excited into the conduction band (CB) are spin polarized [1]. Figure 1 shows a simplified potential energy diagram of a GaAs/vacuum interface. In a simple multiphoton absorption model with an electron affinity of approximately 4.5 eV, a valence band (VB) electron absorbs one 800-nm photon (1.55 eV) to traverse the band gap to the CB. Absorption of two or three more photons provides an electron with energy greater than the electron affinity so it can be directly emitted into the vacuum. Laser pulses of femtosecond duration produced by a mode-locked Ti:sapphire oscillator with a central wavelength of 800 nm generally have enough intensity to make all these processes viable.

In a groundbreaking experiment, Hommelhoff *et al.* used a femtosecond laser to study photoemission from a tungsten field emission tip (FET) [3]. This method was subsequently shown to produce femtosecond electron pulses [4]. In the latter study, using two temporally nonoverlapping laser pulses with a variable delay, it was shown that the electron emission when both pulses were used was the same as the sum of the emissions that each pulse produced individually and was thus additive. If the two nonoverlapping pulses together emitted more electrons than the sum of the individual pulses, they were referred to as "superadditive" and it was shown that this condition indicates a slow process where the electron emission occurs on a time scale qualitatively longer than the pulse widths themselves. It was also observed in Ref. [4] that for time delays $<$ 150 fs, when the two laser pulses were temporally overlapped, they could emit more electrons than would be obtained from summing the output of the individual pulses separated by delays greater than 1 ns. This superadditive behavior, however, is the result not of a slow process but of the constructive interference between the two overlapping laser pulses that increases the rate of multiphoton emission.

In this paper, we employ techniques similar to those used in the examination of FETs, but use a GaAs shard tip as the photoemitter. Figure 2 shows such a shard, similar to the one used in this experiment, that was used in previous work that demonstrated polarized emission from GaAs using the sample's tiplike features [5]. For GaAs with delays greater than 200 fs and less than 1 ns, however, we have now observed that the two nonoverlapping pulses produce fewer electrons combined than the sum of their individual emissions. This phenomenon was not observed with tungsten tips. We refer to it as "subadditivity" and show that it is consistent with a fast electron emission process. In addition, we show that subadditivity is consistent with the promotion of electrons to the GaAs CB due to laser absorption, followed by Pauli blocking of subsequent photon absorption.

Earlier experiments using scanning tunneling microscope (STM) tips to monitor photocurrents from GaAs induced by delayed femtosecond laser pulses have measured a similar

[*]william.newman@huskers.unl.edu
[†]eric.jones@stonybrook.edu
[‡]ebrunkow@southeast.edu
[§]hbatelaan@unl.edu
[‖]tgay1@unl.edu

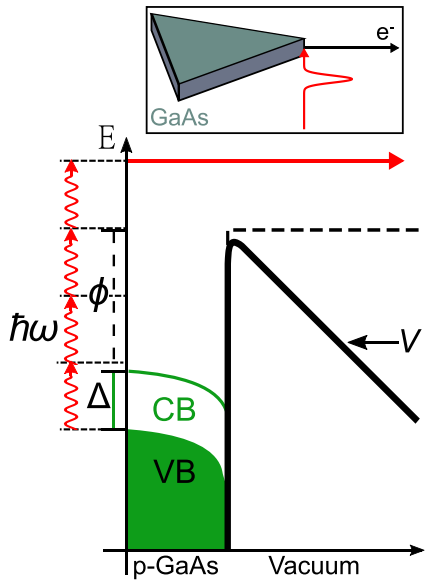

FIG. 1. Pulsed electron multiphoton emission from the apex of a GaAs tip (inset). Each photon has energy $\hbar\omega$, slightly larger than the band-gap energy Δ between the valence band (VB) and conduction band (CB) at the Γ point. The electron can be emitted into the vacuum by exceeding the electron affinity ϕ of GaAs with multiphoton absorption (red arrow) with enhanced emission from the skewed vacuum potential (V) due to electric field effects. The band bending at the surface is due to the p doping typically used for semiconductor photocathodes.

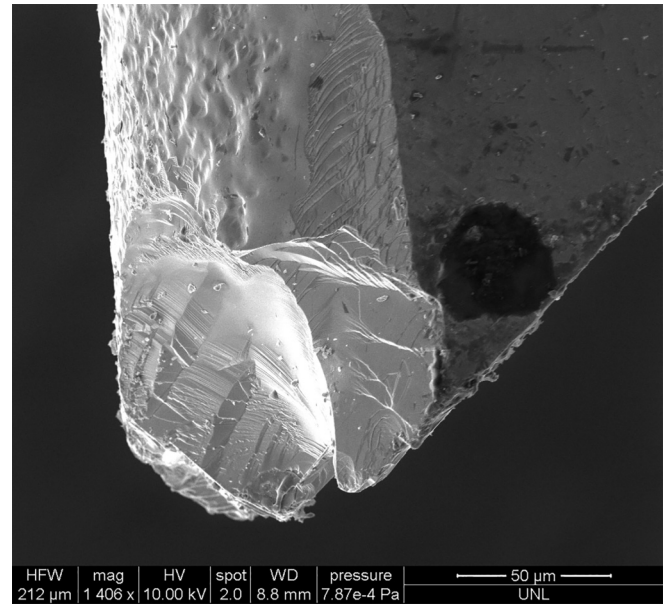

FIG. 2. SEM image of a GaAs shard [5]. The submicron emission sites are located at various points on the shard but primarily towards the apex of the tip. The subadditive behavior occurs primarily for light incident towards the bulk of the shard, as opposed to the sharp features at the apex of the tip.

subadditivity in the photocurrent for laser pulse delays of up to 600 ps [6,7]. Subadditivity in Refs. [6,7] was not investigated further. By observing STM tunneling current during pump-probe experiments in Ref. [7], it was determined that when carriers excited by the first pulse remain in the excited state, the absorption of the second pulse is suppressed. A lifetime for the suppression effect of 440 ps was calculated, which is comparable to the recombination lifetime of bulk-excited electron-hole pairs. However, the emphasis of that experiment was to show the capabilities of a new STM method and no further modeling or experiments were conducted. A similar effect has also been seen in two-photon direct electron emission from Si by an intense laser pulse [8]. If this "probe" pulse was preceded by < 1 ns with a pump pulse with just enough energy to promote VB electrons to the CB, a reduction of the electron emission rate was observed.

To our knowledge, the experiments reported here are the first to observe subadditive effects in direct multiphoton ionization of GaAs. They differ from the Si studies [8] in that they probe only direct band-gap excitation into the CB, making the interpretation and modeling of our results simpler. They are also very sensitive, in that the total electron yield varies by as much as 40%, depending on the pump-probe delay, which is comparable to the largest effects observed in a variety of reflection and transmission pump-probe experiments involving GaAs and its stochastic variants [7,9–22]. Our results are consistent with a simple model of the laser-induced direct band-gap transitions in which the subadditive effect is the result of Pauli blocking caused by the pump laser's excitation of VB electrons, and suggests a strong suppression mechanism for the emission of electrons through saturation of the CB. Our observation of this type of suppression of the emission of electrons from GaAs compliments the many optical studies using similar pump/probe techniques. This suppression of emission following direct band-gap excitation has the potential to allow additional control of the excited and emitted electrons' spin polarization.

II. EXPERIMENT

Broken shards from bulk crystals of 0.3-mm-thick, Zn-doped p-type $\langle 100 \rangle$ orientation GaAs (Crystal Specialists) with dopant carrier concentrations of $\approx 2 \times 10^{19}$ cm^{-3} were used in these experiments. In a first experiment, we used a femtosecond oscillator (KMLabs Griffin) with a nominal wavelength of 800 nm, 30-nm full width at half maximum (FWHM) bandwidth, and 1 nJ/pulse at 90 MHz. These parameters were measured by a combination of a spectrum analyzer (Photon Control), measured power, and intensity read from a fast photodiode which is incorporated in the Griffin optics. We determined that the laser pulse duration is approximately 90 fs, based on the pump-probe analysis outlined below. This is consistent with the standard output parameters for oscillators of this type and is slightly larger than that expected for a transform-limited pulse.

The basic setup for our first experiment is shown in Fig. 3(a). The laser pulses pass through an interferometer that splits them in two. One path is adjustable in length providing spatial and hence temporal separation between the two pulses. The path contains a piezoelectric translation stage which allows delays up to 70 fs and a micrometer-driven stage for delays up to 300 ps. These stages in turn are mounted on a rail that can provide delays greater than 1 ns. The two beams

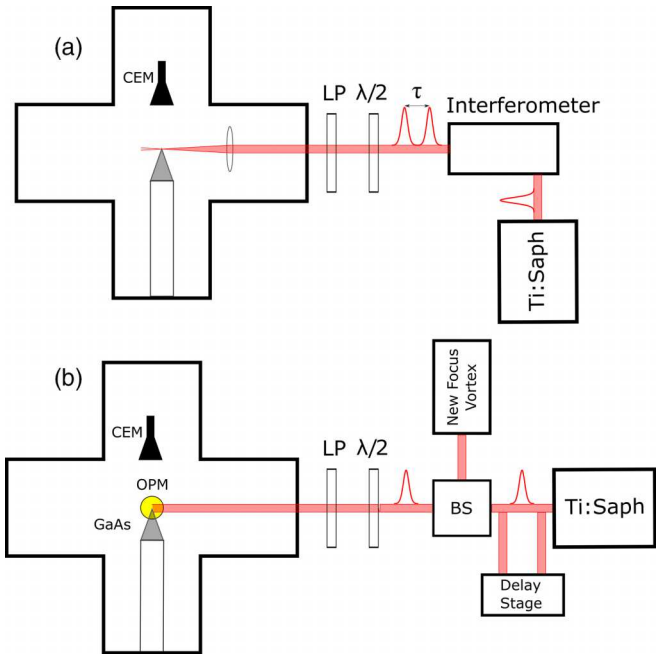

FIG. 3. Schematic of the experimental setups. (a) Pulses from a Ti:sapphire oscillator are split spatially by a Mach-Zender interferometer and delayed by τ to produce the pump and probe pulses. The beam power is adjusted with a half wave plate ($\lambda/2$) and a linear polarizer (LP). A lens in vacuum then focuses the pulses onto the GaAs tip with a $\approx$ 50-μm focal spot radius. The emitted electrons are then counted by a channel electron multiplier (CEM). (b) Pulses from a Ti:sapphire oscillator are aligned with a CW beam of 800-nm light using a beam splitting cube (BS). The experiment had a fixed optional delay ($\tau = 2$ ps) stage which was used to collect the data shown in Fig. 4. These beams are directed by an off-axis parabolic mirror (OPM) to the GaAs tip achieving a focal spot size of $\approx$ 5 μm. Emitted electrons are subsequently counted by a CEM.

travel along different paths and are subsequently recombined collinearly. For large adjustments to the delay arm, the beams were verified to be collinear with a position sensitive detector (On-Trak OT301). The recombined beam had an average power of 50–100 mW, set by a $\lambda/2$ retarder followed by a linear polarizer with a polarization angle aligned with the axis of the tip. It was sent into the vacuum chamber where it passed through a 3.8-cm focal-length lens that focused it down to a $\approx$ 50-μm radius spot.

The GaAs sample is mounted on a three-dimensional translation stage so that it can be moved into and out of the laser focus. How close the sample is to the focus can be determined by looking at the beam after it traverses the chamber and exits through another window. The GaAs tip will partially block the beam, and it can be determined how close to the focus it is by the shadow that it casts on the projection of the beam spot. When in the focus, interference fringes due to diffraction from the crystal edge can be seen. A channel electron multiplier (CEM) sits 2.5 cm from the GaAs. A typical voltage drop from the CEM to the GaAs of 400 V (corresponding to -200 V on the crystal and $+200$ V on the CEM) was used to efficiently collect all of the emitted electrons. Potential differences larger than this did not significantly increase the count rates observed.

To minimize the effect of long-term drift in the count rates, an automated system switched the laser pulse configuration after each electron counting interval. This was accomplished by two stepper motors attached to beam blocks that could be rotated in and out of the two beam paths in the interferometer. Additivity measurements of the electrons emitted by the pump and probe beams involved first having both beams hit the target and counting electrons for 1–10 s, depending on the desired statistical uncertainty. The first beam was then blocked and electrons emitted by the second beam were counted for the same amount of time. Data were then taken with the second beam blocked and the first unblocked. This process was repeated five times for each pump/probe delay. Background count rates were checked on the first and last cycle by blocking both beams.

In a second experimental setup, an 800-nm CW laser beam (New Focus Vortex) was aligned to be collinear with a Ti:sapphire oscillator pulsed beam (Spectra-Physics Tsunami) similar to that employed in the first experiment. The setup for this experiment is shown in Fig. 3(b). The oscillator pulses had a nominal duration of 100 fs, a central wavelength of 800 nm, and a 45-nm FWHM bandwidth, as measured by a frequency-resolved-optical gate (FROG). Its average power was typically 30 mW. Both beams were linearly polarized with polarization angles aligned with the axis of the tip. An off-axis parabolic mirror in the vacuum chamber was used to focus both beams onto the GaAs with a $\approx$ 5-μm-diameter spot size. Additionally, a balanced Mach-Zehnder interferometer allowed for pump-probe scans with delays up to $+/-10$ ps (Thorlabs PE4).

III. RESULTS

To examine the subadditive nature of multiphoton emission from GaAs, we define an additivity ratio,

$$\mathcal{R}(\tau) \equiv \frac{R_{12} - R_1 - R_2}{R_1 + R_2}, \tag{1}$$

where R_{12}, R_1, and R_2 are the electron count rates for when both pulses, the pump pulse, or the probe pulse, respectively, are incident on the crystal. In the first case, the time delay between the two pulses is τ. The electron emission process is additive when $\mathcal{R}(\tau) = 0$, superadditive when $\mathcal{R}(\tau) > 0$, and subadditive when $\mathcal{R}(\tau) < 0$.

Since the emission process requires at least three photons, the emission is most likely to occur for locations in the focus where the intensity is the highest. We found that the subadditive effect occurred predominantly when the GaAs tip was in the laser's focal plane with an overlap of about 3 μm or about half of the laser's total diameter (Fig. 4). The data of Fig. 4 were taken with a pump-probe delay of 2 ps, which is roughly (on a log scale) in the middle of the temporal delay region for which subadditivity is observed (see Fig. 5). These data were obtained using the setup shown in Fig. 3(b) with a fixed delay arm added and no CW laser. As the tip is moved deeper into the focus, the photoemission rate peaked and then fell to very low levels, indicating that while the free electron production process is associated with bulk material, these free electrons are most readily emitted in the vicinity of the tip, where surface fields are much higher [3].

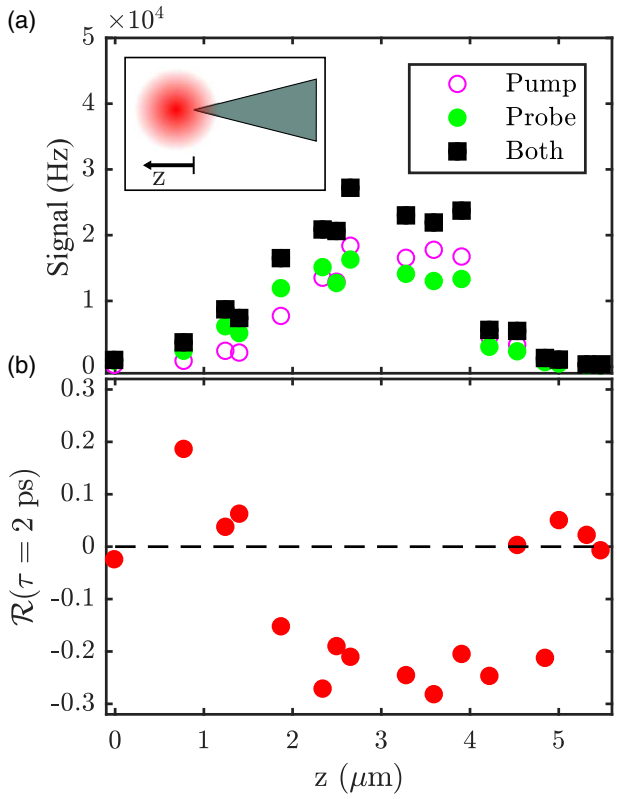

FIG. 4. Electron emission rates for the individual and combined beams and the additivity ratio, $\mathcal{R}(\tau = 2$ ps), as defined by Eq. (1), vs the position of the laser's focal spots on the GaAs tip. (a) Electron counts obtained from the pump (magenta open circles), probe (green circles), and both (black squares) beams incident on the sample, for approximately 9 mW of incident power per beam. The $z = 0$ position is taken to be the axial coordinate of the tip when electron emission is first observed, although, given the nonlinearity of the photoemission process, this position may still be associated with a significant photon flux. (b) $\mathcal{R}(\tau = 2$ ps) vs position. When the tip is translated further into the focus, the subadditive effect becomes stronger. This suggests that the cause of subadditive emission is due to processes occurring within the bulk of the tip samples. These data were taken using the apparatus shown in Fig. 3(b).

For small $\tau < 100$ fs, the laser pulses largely overlap in time where they constructively and destructively interfere, resulting in a rapidly oscillating count rate as seen in Fig. 6. When these pulses interfere maximally $\mathcal{R}(\tau)$ can be as large as 7, 31, and 127 for a two-, three-, or four-photon process respectively. The data shown in Fig. 6 thus appear to be most consistent with a three-photon process. Our model incorporates both three- and four-photon processes that simulate the data well. Justification of the inclusion of these dual processes and how they are implemented in the model is discussed later in the text. For longer time delays between 200 fs and 1 ns, $\mathcal{R}(\tau)$ becomes negative, stays negative, and then approaches zero, as shown in Fig. 5. We show below that the time structure of this subadditivity is the result of a combination of electron thermalization and electron-hole recombination rates in GaAs.

A second experiment [Fig. 3(b)] was carried out using a CW laser and a pulsed laser. We define the CW additivity ratio as

$$\mathcal{R}_{\mathrm{CW}} \equiv \frac{R_{\mathrm{on}} - R_{\mathrm{off}}}{R_{\mathrm{off}}}, \tag{2}$$

where R_{on} (R_{off}) is the emission rate when the pulsed laser is on and the CW laser is on (off). The experimental data of Fig. 7 show that $\mathcal{R}_{\mathrm{CW}}$ is essentially linearly dependent on CW power. This indicates that the population of the CB must affect $\mathcal{R}_{\mathrm{CW}}$ as the CW beam can only excite electrons across the band gap.

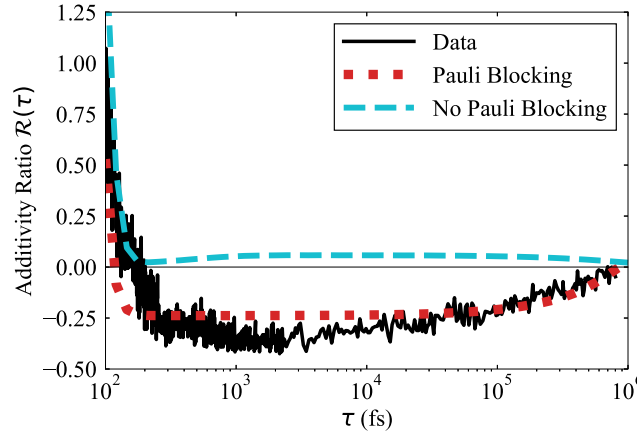

FIG. 5. $\mathcal{R}(\tau)$ for $\tau > 100$ fs. The experimental data (black), taken with the apparatus shown in Fig. 3(a), are compared to our model calculations with (red dotted) and without (blue dashed) the Pauli blocking term. The subadditive dip begins at $\tau = 200$ fs and persists until 1 ns. The inclusion of Pauli blocking is essential to describe the subadditive effect for these data.

IV. MODEL

We discuss here a model that describes the multiphoton emission of electrons from the GaAs VB into the vacuum.

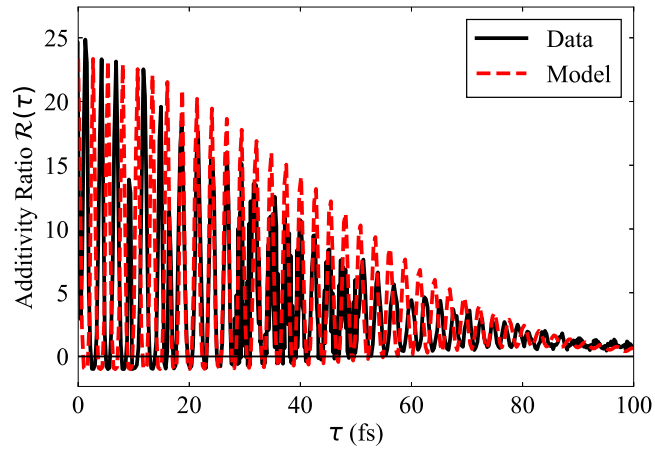

FIG. 6. An autocorrelation curve, taken with the apparatus shown in Fig. 3(a), for $\mathcal{R}(\tau)$ when $\tau < 100$ fs and the pump and probe pulses overlap in time and space. Our model results (discussed in Sec. IV) have a somewhat larger amplitude than the data when Pauli blocking is included. When Pauli blocking is excluded (not shown due to scale), the peak amplitude reaches a value of 80.

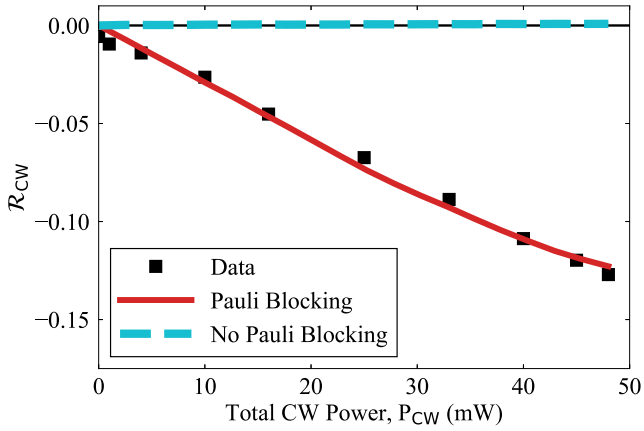

FIG. 7. The additivity ratio R_{CW} for the combination of pulsed and 800-nm CW laser beams incident on the GaAs sample, measured with the apparatus shown in Fig. 3(b). As the CW laser power is increased, the emission due to the pulsed beam decreases in a quasi-linear fashion. The blue dashed curve shows the model's prediction when Pauli blocking is excluded.

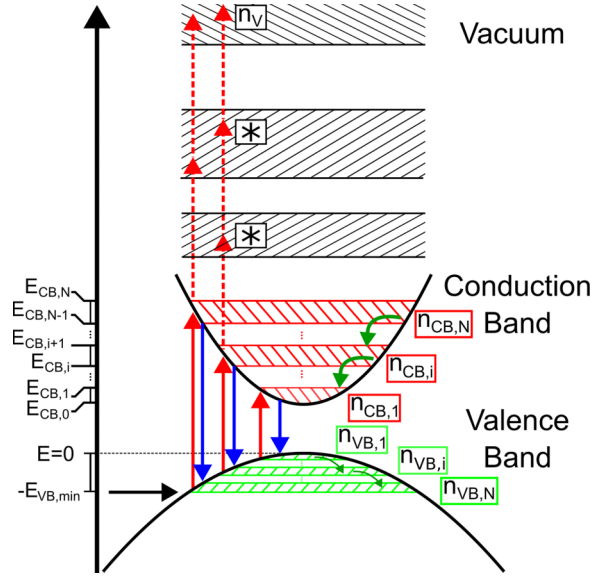

FIG. 8. Energy level diagram relevant for subadditive multiphoton emission from GaAs. Laser pulses drive single photon direct transitions (red arrows) from energetically accessible regions of the valence band (VB) having $N = 28$ population sublevels $n_{VB,1}, n_{VB,2}, \ldots, n_{VB,28}$ to the corresponding regions of the conduction band (CB) with energies ranging from $-E_{VB,min}$ to $E = 0$, where $E_{VB,min}$ corresponds to the lowest energy accessible as determined by the energy bounds in the pulse's photon distribution (see Fig. 9). The CB has sublevel populations $n_{CB,1}, n_{CB,2}, \ldots, n_{CB,28}$, with the maximum energies of the CB subband populations $E_{CB,i}$ given by $E_{CB,i} = E_{CB,0} + i\delta E$, where $E_{CB,0} = 1.34$ eV is the band-gap energy and $\delta E = 0.0125$ eV. Electrons from higher-energy CB sublevels ($n_{CB,i}$) can thermalize (green arrows) into lower-energy sublevels ($n_{CB,i-1}$). The VB sublevels thermalize in a similar manner with $n_{VB,i+1}$ lying at a lower energy than $n_{VB,i}$. Electrons can fill the energy states of the CB until a threshold value unique to each level, $N_{CB,i}$, is reached (see Fig. 9). Similarly, the VB sublevels start at a maximal value $N_{VB,i}$ and can be replenished through diffusion (black arrow), thermalization (green arrows), or electron-hole recombination (blue arrows). Electrons are emitted after the absorption of two or three additional photons (dashed red arrows) through one or two virtual states (∗) into the vacuum state (n_V) for the three- and four-photon emission processes.

We have tried to keep it as simple as possible while still including all of the physical processes necessary to comprehensively and consistently describe the subadditive effects we observe. What appear to be nonessential processes, interactions, or mathematical descriptions that provide only marginal improvements of the model's fits to the data have been ignored in this first-order approach. The neglected processes and their influence on our results are discussed, where appropriate, throughout the section.

The model is based on $2N + 1$ coupled population levels of the GaAs bulk and vacuum, as shown in Fig. 8. The single pulse electron emission was observed to depend on the fourth power of intensity in experiments related to this paper, but in our model we have assumed both three- and four-photon absorption in the emission rate calculations [23]. In general, the photon order of a nonlinear process can be determined from autocorrelation curves like that shown in Fig. 6 by examining the ratio of the peak widths and the peak-to-peak separation. The experimental data in Fig. 6 show ratios that are consistent with both four- and three-photon emission processes. The energetically accessible $N = 28$ VB population sublevels ($n_{VB,1} \ldots n_{VB,28}$) are allowed to be directly excited to $N = 28$ CB population sublevels ($n_{CB,1} \ldots n_{CB,28}$) after absorbing one photon, or to be excited to the vacuum population level (n_V) through the virtual states (*) through three- or four-photon absorption. Electrons can also be excited into the vacuum level from the CB levels through the virtual states after absorbing two or three photons. Our model ignores indirect phonon-coupled processes.

The transitions to the CB population levels are governed by the incident photon energy distribution, where the transition to the ith sublevel corresponds to photons with the required energy, $E_{\gamma,i}$, for such an excitation. The photoexcitation rates for each sublevel include a multiplicative factor, α_i (Fig. 9), as the fraction of photons in the laser pulse that have the appropriate energy to excite a direct transition from the VB sublevel $n_{VB,i}$ to the CB sublevel $n_{CB,i}$ (Fig. 8). All of the pulsed-laser photons can directly excite one of the partitioned energy levels of the CB, but the majority of them cause transitions in the energy range of 1.45–1.66 eV with 1.34 eV being the energy of the transition at the $k = 0$ Γ point. (The Γ-point gap is 80 meV less than that of pure GaAs because of the large p-doping concentrations of the GaAs crystal used in this paper [24].) The number of sublevels, N, was chosen to be 28, which represents a compromise between accurate representation of the energy distribution of the incident photon pulses, the density-of-states variation with energy in the CB, and computational tractability.

The stimulated emission and multiphoton excitation probabilities also depend on the time-dependent factors γ and $\omega_{o,f}$, where o and f indicate the initial and final states of the transition. These factors will be described below. Each CB sublevel can also gain electrons from immediately adjacent higher-energy CB states through a thermalization process,

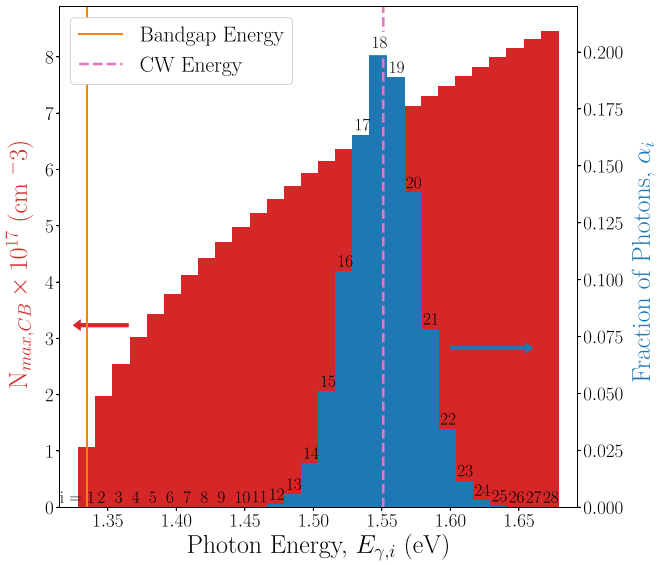

FIG. 9. A normalized discrete Gaussian distribution (blue), representing the photon energy distribution of a pulse of light centered at $\lambda = 800$ nm with a FWHM of 30 nm, and a histogram of the maximum population values $N_{\mathrm{CB},i}$ for the CB sublevels with their corresponding indices, $i = 1$–28 (red; see text). The orange solid line shows the minimum band-gap energy necessary for transitions to the CB from the VB, and the magenta dotted line shows the CW laser energy which coincides with the center wavelength of the laser pulses. The $N = 28$ bins are used to estimate the fraction of photons, α_i, with energy $E_{\gamma,i}$, that are capable of directly exciting electrons from the VB to the CB sublevels with the required amount of energy (see Fig. 8). Photon populations in the pulse's "wings" (bins 1–11 and 26–28) are small but non-negligible. The energy values from the photon energy distribution are used in Eq. (7) to estimate the maximum population values, $N_{\mathrm{CB},i}$, for each sublevel population.

or lose electrons to immediately adjacent lower-energy CB states by thermalization or to the VB via spontaneous or photon-stimulated electron-hole recombination. The thermalization rate, $\Gamma_{\mathrm{CB},T}$, which depends on the frequency of excited electron collisions with other electrons or the GaAs lattice (phonon production and scattering), has a best fit value of 33 ns^{-1} for the data shown in Figs. 5 and 7. This corresponds to a thermalization lifetime of 30 ps and is significantly larger than those measured in many previous pump/probe reflection/transmission measurements, but is essential to obtain agreement with the data of Figs. 5 and 7 [10–20]. We note, however, that a longer lifetime of 100 ps has been observed for energetic electron decay within the CB of cold-grown GaAs [25,26]. This reduced interaction gives a smaller cooling rate resulting in photoinjected electrons taking longer to equilibrate to lattice temperatures. Additionally, with the GaAs tip at room temperature and with excitation energies higher than the CB minimum, the thermalization of electrons will contribute to the phonon bath which could in turn excite electrons, increasing the thermalization lifetime [18]. With LO phonons in GaAs having a typical energy of about 36 meV and our CB sublevels having a width of 12.5 meV, electrons decaying from high-energy states to low-energy states would actually cross multiple levels [10]. In our nearest-neighbor transition model, this effect is accounted for in the value of $\Gamma_{\mathrm{CB},T}$. All transitions or decays to the CB sublevels are suppressed by a population dependent factor $f(n_i)$ that quantifies the blocking effect of the Pauli exclusion principle described below.

Similarly to the CB, each VB sublevel can gain electrons from nearest-neighbor sublevel populations via hole thermalization with rate $\Gamma_{\mathrm{VB},T}$, or from the bulk through hole diffusion with rate Γ_D. The values of $\Gamma_{\mathrm{VB},T}$ and Γ_D are obtained from the literature with values 8 and 0.7 ps^{-1} respectively [21,27]. The VB (CB) also gains (loses) electrons through electron-hole recombination, with a fitted value of $\Gamma = 1$ ns^{-1}, in close agreement with other calculated values [7,9,10,17]. A summary of the terms included in the rate equations and their physical significance is given in Table I with a detailed discussion of their formulation below.

The rate equations for the ith VB and CB sublevel population as well as the vacuum population level are

$$\frac{dn_{\mathrm{VB},i}}{dt} = -\omega_{\mathrm{VB},V}\, n_{\mathrm{VB},i}\, \alpha_i\, f(n_{\mathrm{CB},i}) - \gamma\alpha_i\, n_{\mathrm{VB},i}\, f(n_{\mathrm{CB},i}) + \gamma\alpha_i\, n_{\mathrm{CB},i}\, f(n_{\mathrm{VB},i}) + \Gamma\, n_{\mathrm{CB},i}\, f(n_{\mathrm{VB},i}) + \Gamma_D\, (N_{\mathrm{VB},i} - n_{\mathrm{VB},i})$$
$$+ \Gamma_{\mathrm{VB},T}[n_{\mathrm{VB},i-1}\, f(n_{\mathrm{VB},i})(1-\delta_{i,N}) - n_{\mathrm{VB},i}\, f(n_{\mathrm{VB},i+1})(1-\delta_{i,1})], \tag{3a}$$

$$\frac{dn_{\mathrm{CB},i}}{dt} = \omega_{\mathrm{VB},V}\, n_{\mathrm{CB},i}\, \alpha_i\, f(n_{\mathrm{CB},i}) - \omega_{\mathrm{CB},V}\, n_{\mathrm{CB},i} + \gamma\alpha_i\, n_{\mathrm{VB},i}\, f(n_{\mathrm{CB},i}) - \gamma\alpha_i\, n_{\mathrm{CB},i}\, f(n_{\mathrm{VB},i}) - \Gamma n_{\mathrm{CB},i}\, f(n_{\mathrm{VB},i})$$
$$+ \Gamma_{\mathrm{CB},T}[n_{\mathrm{CB},i+1}\, f(n_{\mathrm{CB},i})(1-\delta_{i,N}) - n_{\mathrm{CB},i}\, f(n_{\mathrm{CB},i-1})(1-\delta_{i,1})], \tag{3b}$$

$$\text{and} \quad \frac{dn_V}{dt} = \omega_{\mathrm{VB},V} n_{\mathrm{VB}} \left(\sum_{i=1}^{N} \alpha_i f(n_i) \right) + \omega_{\mathrm{CB},V} \sum_{i=1}^{N} n_i, \tag{3c}$$

where $\delta_{j,i}$ is the Kronecker delta function and is included to correct the thermalization terms at the highest- and lowest-energy population sublevels.

We assume an equivalent cross-sectional value for all single photoexcitations in the system. The single photon absorption rate is described by

$$\gamma = A[\hat{E}_{\mathrm{pump}}(t) + \hat{E}_{\mathrm{probe}}(t-\tau)]^2, \tag{4}$$

where A is a constant that incorporates, among other constants, the photon flux and the single photoexcitation cross

TABLE I. Rate terms that construct the $2N+1$ rates of Eq. (3). These terms exist in Eq. (3) as either an addition or subtraction to the population rate equations. The individual factors given in these terms are explained in the text.

Rate term	Description
$\omega_{\mathrm{VB},V}\ n_{\mathrm{VB},i}(\sum_{i=1}^{N}\alpha_i f(n_i))$	Multiphoton excitation from $n_{\mathrm{VB},i}$ to n_V
$\gamma\ n_{\mathrm{VB},i}\ \alpha_i f(n_{\mathrm{CB},i})$	Single photon excitation from $n_{\mathrm{VB},i}$ to $n_{\mathrm{CB},i}$
$\gamma\ \alpha_i\ n_{\mathrm{CB},i}$	Stimulated emission from $n_{\mathrm{CB},i}$ to $n_{\mathrm{VB},i}$
$\omega_{\mathrm{CB},V}\ n_{\mathrm{CB},i}$	Multiphoton excitation from $n_{\mathrm{CB},i}$ to n_V
$\Gamma\ n_{\mathrm{CB},i}$	Electron-hole recombination from $n_{\mathrm{CB},i}$ to $n_{\mathrm{VB},i}$
$\Gamma_{\mathrm{CB},T}\ n_{\mathrm{CB},i}\ f(n_{\mathrm{CB},i-1})$	Thermalization of electrons from $n_{\mathrm{CB},i}$ to $n_{\mathrm{CB},i-1}$ with $n_{\mathrm{CB},i-1}$ lying at a lower energy than $n_{\mathrm{CB},i}$
$\Gamma_{\mathrm{VB},T}\ n_{\mathrm{VB},i}\ f(n_{\mathrm{VB},i+1})$	Hole thermalization from $n_{\mathrm{VB},i+1}$ to $n_{\mathrm{VB},i}$ with $n_{\mathrm{VB},i+1}$ lying at a lower energy than $n_{\mathrm{VB},i}$
$\Gamma_{\mathrm{VB}}(N_{\mathrm{VB},i}-n_{\mathrm{VB},i})$	Hole diffusion into the bulk from $n_{\mathrm{VB},i}$

section. The explicit time dependence of γ is given by the square of the sum of the dimensionless electric field terms, $\hat{E}_{\mathrm{pump}}$ and $\hat{E}_{\mathrm{probe}}$, each having the same amplitude. These have the chirped Gaussian form $\exp(-\frac{t^2}{2\sigma_t^2})\cos(\omega_c t + bt^2)$, where σ_t is the temporal width of the Gaussian profile pulse at half maximum, ω_c is its central frequency corresponding to a central wavelength of 800 nm, and b is a linear chirp coefficient. The chirp coefficient ($b = 3.41 \times 10^{26}\ \mathrm{s}^{-2}$) is included to obtain a better fit to the data for $\tau < 200$ fs (Figs. 5 and 6) when the pulses overlap and shortly after, but does not significantly affect the model results for $\tau > 200$ fs shown in Fig. 5. In our model, γ describes the single photon excitation rate as well as the rate of stimulated decay. We then can write the multiphoton absorption rates as [28]

$$w_{\mathrm{VB},V} = \beta\gamma^4\Delta t\tau_*^2 + \kappa\gamma^3\Delta t\tau_* \tag{5a}$$

$$\text{and} \quad w_{\mathrm{CB},V} = (\beta\gamma^3\tau_*^2 + \kappa\gamma^2\tau_*)/\chi, \tag{5b}$$

where τ_* is the lifetime of the transient state $*$; Δt is the laser pulse duration, 90 fs; and β and κ are proportionality constants for four- and three-photon emission rates with values of 0.997 and 0.003 respectively. Both β and κ are fitted to maximize agreement with the experimental data in Fig. 6. It was found that the three-photon process contributes little to the overall emission. The factor χ is a heuristic constant in order to obtain agreement for the data in Fig. 5; without it the overall additivity ratio increases positively both with and without Pauli blocking. We find the best fit to the data of Fig. 5 with $\chi = 4.7$. The value of τ_* is estimated through the uncertainty principle to be $\hbar/E_\gamma$, with $E_\gamma = 1.55$ eV, so $\tau_* = 0.4$ fs. To accurately describe the resonantly enhanced emission process, Δt is used for the transient lifetime of the CB in Eq. (5a), since a CB electron is only limited to the duration of the laser pulse for further excitation [29]. Higher-lying CB states of GaAs have been predicted, assuming an infinite crystal, to exist at the Γ point about 4.5 eV above the top of the VB [30]. Their exact character, though, is unclear given that in a real crystal they would be indistinguishable from some combination of surface states. We attempted to include such a real level in our model, but it led to a variety of results that bore no resemblance to our experimental data.

The effect of Pauli blocking on any population increases to the CB and VB sublevels and is included in the model by considering a linear population-dependent function, $f(n_i)$, that increasingly blocks excitation or decay to the ith sublevel as n_i reaches a maximum population value $N_{\mathrm{CB},i}$ for the CB and $N_{\mathrm{VB},i}$ for the VB: $f(n_{\mathrm{CB/VB},i}) = (1 - n_{\mathrm{CB/VB},i}/N_{\mathrm{CB/VB},i})$. As the CB or VB sublevel populations increase, the number of available states decreases by a factor of $n_{\mathrm{CB/VB},i}/N_{\mathrm{CB/VB},i}$ which limits the probability of a transition. Only the suppression terms for the CB are removed for cases where Pauli blocking is absent from the model (see Figs. 5 and 7).

The value of $N_{\mathrm{CB},i}$ is estimated as the maximum carrier density in each CB sublevel taken from the filled-hole density ($N_{\mathrm{VB},i}$) in the VB sublevel, with explicit forms of [31]

$$N_{\mathrm{VB},i} = \frac{m_{\mathrm{VB}}^{3/2}}{\hbar^3\pi^2}\int_{E_{\mathrm{CB},0}-E_{\mathrm{CB},i+1}}^{E_{\mathrm{CB},0}-E_{\mathrm{CB},i}} dE\sqrt{-2(E - E_{\mathrm{CB},0} + E_{\mathrm{CB},i})} \tag{6}$$

and

$$N_{\mathrm{CB},i} = \frac{m_{\mathrm{CB}}^{3/2}}{\hbar^3\pi^2}\int_{E_{\mathrm{CB},i}}^{E_{\mathrm{CB},i+1}} dE\sqrt{2(E - E_{\mathrm{CB},i})}, \tag{7}$$

where $E_{\mathrm{CB},0}$ is the band-gap energy at the Γ point. The bounds of integration for Eqs. (6) and (7) are determined by the range of photon energies that can excite the ith CB sublevel from the energetically available ith VB sublevel (see Figs. 8 and 9). The CB and VB carrier masses are given as $m_{\mathrm{CB}} = 0.066\,m_e$ and $m_{\mathrm{VB}}^{3/2} = m_{\mathrm{LH}}^{3/2} + m_{\mathrm{HH}}^{3/2}$, where m_{HH} and m_{LH} are the heavy-hole and light-hole masses and are taken to be $0.6\,m_e$ and $0.07\,m_e$ respectively [22]. The 28 CB sublevel population maxima are shown in Fig. 9. The initial VB sublevel populations are calculated in a similar manner with sublevel energy ranges decreasing with increasing index.

The use of Pauli blocking to describe suppression has been considered extensively elsewhere in the context of electronic excitation in semiconductors (see, e.g., Refs. [7,8,32]). The Pauli blocking term $f(n_i)$ is essential to describe the subadditive effect we observe for the data of Figs. 5–7. When this term is neglected in the model, the subadditive effect is completely eliminated and actually becomes superadditive, as seen in Fig. 5. We also note that the number density of free electrons excited by each laser pulse, as inferred from Fig. 10, is of the order of $10^{17}\ \mathrm{cm}^{-3}$, which is comparable to the densities considered in other work [13,15,16,33].

The behavior of the CB sublevel populations is influenced by the various decays and excitations that occur, with their cumulative effects shown in Fig. 10. The population increase

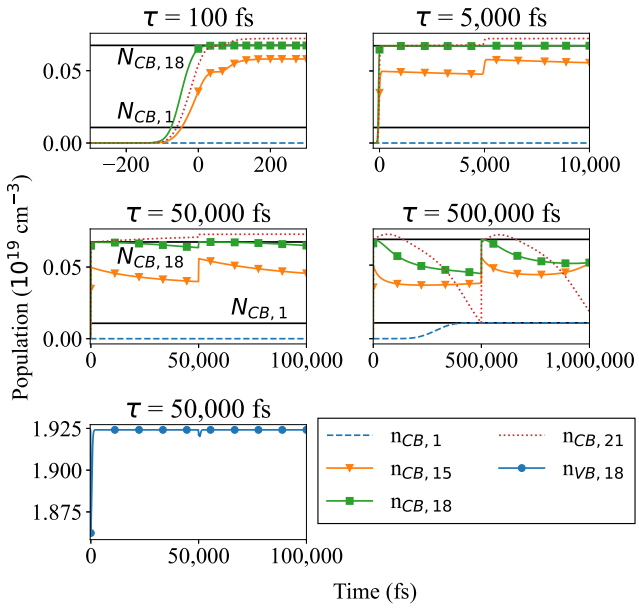

FIG. 10. The top four plots show various CB sublevel populations over increasing time scales with both the pump and probe pulses causing excitations. Each plot is for a different time delay ranging between 100 and 5×10^5 fs. The various decay dynamics of the CB sublevel populations can be seen for all the time delays. The CB sublevels reach maximum values and start to decay as electrons recombine with holes in the VB as well as thermalize into lower-energy CB sublevels. The maximum values for $N_{\mathrm{CB},18}$ and $N_{\mathrm{CB},1}$ are indicated by the horizontal black lines. The bottom plot shows the $N_{\mathrm{VB},18}$ population level for comparison with the 5×10^4 fs time delay plot immediately above it.

due to photon absorption is largest for the $n_{\mathrm{CB},18}$ population and decreases for sublevels further away in energy, as is expected with the photon distribution factors α_i shown in Fig. 9. While the population increase due to absorption is roughly symmetric about the $n_{\mathrm{CB},18}$ population, the population values for delays $\gtrsim$20 ps become more asymmetric due to thermalization in the CB. Populations at these intermediate delay times are largely governed by the thermalization and electron-hole recombination rates, whose values strongly affect the model predictions for the shape of the subadditivity curve for delay times $> 1 \times 10^4$ fs in Fig. 5. Longer thermalization lifetimes extend the subadditive behavior beyond $\tau > 1$ ns. The VB population for the $i = 18$ sublevel is shown in Fig. 10 and demonstrates that the most extreme decrease in the VB sublevel populations is about 5%.

The constant A introduced in Eq. (4) can be estimated by using a photon flux distribution that produces the observed electron count rate R_e for a single pulse incident on the GaAs sample in the experimental setup shown in Fig. 3(a). The photon flux is determined from the measured laser pulse energy and an estimation of the total area of our GaAs sample that is under laser illumination. The measured average powers of our pump and probe beams in the pulsed experiment were between 50 and 100 mW which, for our oscillator operating at a repetition rate of 90 MHz, gives a pulse energy of $E_{\mathrm{pulse}} = 0.6$–1.2 nJ. The total number of photons in each pulse is estimated by $M = E_{\mathrm{pulse}}/\hbar\omega$, where $\hbar\omega = 1.55$ eV for 800-nm light. The beam area is $\pi w_o^2/2$, where w_o is the waist diameter of a Gaussian beam at the focus, measured to be 50 μm. However, as the GaAs tip does not intercept every photon in the beam, emission proceeds from particularly sharp "hot spots" at the apex [5]. To account for this, the beam area is adjusted to 1% of its nominal value resulting in an effective area $A_{\mathrm{eff}} = 8.5 \times 10^{-9}$ cm^2, and the effective number of photons per pulse, M_{eff}, is computed with respect to that portion of the beam. With this A_{eff}, an initial VB electron density ρ of 9.5×10^{18} cm^{-3} [34], and a photon penetration depth δ of 0.75 μm [35], the initial number of electrons available for excitation is approximately $R_o = A_{\mathrm{eff}}\delta\rho = 6.1 \times 10^6$. The yield of emitted electrons is then estimated from the ratio of the electron count rate to the repetition rate of the laser and varies from 10^{-1} to 10^{-3} electrons per laser pulse. The four-photon ionization process from the VB is much more significant than the multiphoton processes of three-photon ionization from the VB and ionization from the CB due to the factor κ and the relatively low population value of the CB sublevels respectively (see Fig. 10).

The observed single-pulse electron emission rate is thus

$$R_e = R_o \int_{\mathrm{pulse}} dt\, \omega_{\mathrm{VB},V}. \tag{8}$$

Using Eqs. (5b) and (4), we find the estimate of A to be

$$A = \frac{\sigma M_{\mathrm{eff}}}{A_{\mathrm{eff}}} \frac{1}{\sqrt{\pi\sigma_t^2}}, \tag{9}$$

where σ is the estimated cross-sectional value for single photon absorption. Using Eqs. (5b), (8), and (9) where only four-photon processes and the values of the constants therein are considered, the value of σ is estimated to range between $4 - 22 \times 10^{22}$ cm^2, yielding values of A ranging from $0.3 - 3.8 \times 10^{11}$ s^{-1}.

When implementing the model, the best fit for the subadditive data represented in Fig. 5 occurred for a model coefficient $A = 2.4 \times 10^{13}$ s^{-1}. This is much larger than the above estimates but is necessary to achieve the large subadditive depth seen in Fig. 5. With larger or smaller values of A the depth of the subadditive effect becomes stronger or weaker respectively. Similarly, for the short delays seen in Fig. 6, the value of A affects the value of the peak amplitude when the pulses temporally overlap. While both attributes are affected by the value of A, $\mathcal{R}(\tau)$ for 200 fs $\leqslant \tau \leqslant$ 1 ns is most sensitive to this constant. Additionally, when Pauli blocking is removed the model predicts extremely large additivity ratios at the peak amplitude with a value of 80. This is less than the theoretical value for a four-photon process, 127, which can be attributed to a partial bleaching of the valence band. The large difference in amplitudes shows the importance of Pauli blocking in the CB sublevel states.

To model the data shown in Fig. 7, we include the one photon excitation rate due to the CW laser:

$$\omega_{\mathrm{CW}} = A_{\mathrm{CW}} P_{\mathrm{CW}}, \tag{10}$$

where A_{CW} is a constant and P_{CW} is the measured CW laser power. The CW laser photon energy of 1.55 eV excites electrons from the VB to the $i = 18$ sublevel of the CB in our model. Thus stimulated decay from the CB

due to the CW laser occurs for this level. These additional rates modify Eq. (3a) with a subtraction and addition of $\omega_{CW} n_{VB,18} f(n_{CB,18})$ and $\omega_{CW} n_{CB,18} f(n_{VB,18})$ respectively, with corresponding changes to the rate equation for the $i = 18$ CB sublevel population. The value of A_{CW} is estimated as $(1 \times 10^{-6}\ \mathrm{mW}^{-1})A$ to provide the best fit with the experimental data shown in Fig. 7. The data in Fig. 7 are simulated by considering excitation from two pulses separated by 11 ns which corresponds to the repetition rate of the pulsed laser while the CW excitation occurs. Without the Pauli blocking term, R_{CW} increases but at a small rate with a maximum value of 8×10^{-4}. The model-predicted values of R_{CW} are heavily influenced by nearly all of the fitted parameters in our model with the shape of the curve being primarily affected by $\Gamma_{CB,T}$ and A_{CW}.

The effects of the thermalization and diffusion of holes in the VB have a very weak effect on the model results. As indicated in Fig. 10, the VB sublevel populations do not diminish appreciably, with roughly a 5% decrease for the $n_{VB,18}$ sublevel population where the photon distribution has a maximum number of photons. Other sublevels exhibit smaller maximal decreases. Thus bleaching of the VB is not a significant factor in the reduced emission of electrons predicted by the model. This is clearly indicated by the lack of subadditivity when Pauli blocking is removed from the model for long time delays as seen in Fig. 5, as well as by the effect of Pauli blocking on the population of the CB sublevels as seen in Fig. 10.

V. DISCUSSION AND CONCLUSION

Figure 5 illustrates nicely the transition of GaAs multiphoton electron emission from a condition of superadditivity, corresponding to short time delays where the pump and probe laser pulses overlap and interfere constructively, to subadditivity at longer time delays, where photoemission caused by the probe pulse is reduced by Pauli blocking by the CB. Without Pauli blocking, our model predicts superadditivity ($\mathcal{R} > 0$) of the photoemission for delays greater than 200 fs. This is different from results for W tips [4], in which additive electron emission was observed for delay times corresponding to no laser pulse overlap. Such additivity implies that the electron pulses are emitted independently of each other, and are of comparable duration to the photon pulses. As such, the emission process is fast. The subadditivity due to Pauli blocking in our case demonstrates that the emitted electron pulses are independent and the emission process is fast as well. Since Pauli blocking is not operational in the W case, those results were additive for the largest time delays they investigated: 175 fs.

The photoelectron emission from GaAs exhibits subadditive behavior for time delays of the pump and probe pulses from 200 fs up to 1 ns. Pump/probe analysis of multiphoton emission from GaAs has not been carried out to date and complements the many optical studies using pump/probe techniques [7,9–22]. While similar to the work in Ref. [8], where large effects in the reduction of electron emission in silicon were seen over a limited range of electron emission energies, our experiments demonstrate emission reduction as large as 40% for the total electron yield. The superadditive and subadditive behaviors we observe are modeled with good qualitative agreement assuming direct electronic excitation of bulk GaAs, taking into account multiphoton excitation, electron-phonon and/or electron-electron thermalization, and spontaneous and stimulated decay of the excited CB electrons. We infer from this that the subadditive effect in multiphoton emission is due to the inhibition of excitation from the VB due primarily to Pauli blocking by electrons excited to the CB by the pump pulse.

This subadditive effect could possibly be explained by other means as well. One such method is surface photovoltage (SPV) effects. The SPV effect is a well-known method of studying surface and bulk electronic-state information in semiconducting materials by producing photoexcited electrons and measuring the induced surface voltage changes at surface-vacuum and semiconductor-metal interfaces [36]. The theory of SPV effects provides an excellent description for GaAs samples under illumination, as shown in Liu *et al.* [37]. Additionally, the SPV effect has been used to study effects on deep electronic states of GaAs in the ultrafast regime [38]. In connection with the results shown here, illuminating the GaAs tip source in this experiment could exhibit a significant SPV effect. This effect could change the emission of electrons from the probe pulse after illumination from the pump pulse. However, due to the nature of the experiment a good description of any SPV would be fundamentally difficult; SPV is heavily dependent on the surface geometry and in our experiment the surface is ill defined. While SPV effects may contribute to the results presented in Figs. 5 and 6, we expect them to have a relatively small influence. Increasing the attracting potential of the CEM in the experiment shown in Fig. 3(a) did not increase the overall observed count rate, suggesting that any postemission field effects from SPV are overwhelmed by the CEM's bias. Any SPV effects contributing to our results must thus be due to an influence on the electron transport in the emission process through the energy-band bending at the surface. The same lack of effect upon increasing the CEM attracting potential was not confirmed in the experiments done using the CW laser [Fig. 3(b)].

The explanation of subadditivity by Pauli blocking suggests a promising application regarding the production of spin-polarized electrons from GaAs photoemitters. Figure 7 shows that the electron emission rate can be suppressed with a linear dependence on the CB population by using a suitable CW laser at the appropriate wavelength. Circularly polarized

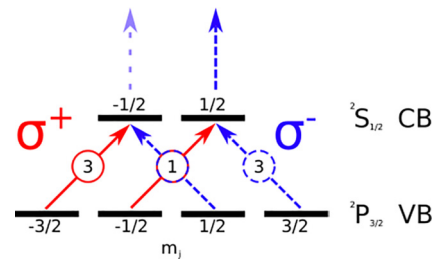

FIG. 11. An illustration of the transitions for CW and pulsed laser light near the band-gap energy with opposite helicities, σ^+ and σ^- respectively, and their relative probabilities from angular momentum selection rules. The upper arrows demonstrate a suppression of emission from the $-1/2$ spin state channel.

lasers induce transitions to the CB at different rates based on angular momentum selection rules as shown in Fig. 11 [1,2]. Electrons emitted by a properly polarized pulsed laser are expected to experience varying degrees of suppression depending on the relative polarizations of the CW and pulsed lasers. The spin lifetime in the CB is expected to be on the order of 0.1 μs which is much longer than the electron-hole recombination lifetime. While it does not affect results reported here, it would in this proposed method [39]. This level of control of subadditivity by CW laser power, shown in Fig. 7, suggests an easy-to-implement tunability of the polarization of electrons excited to the CB and vacuum with this laser configuration. The prospect of a tunable, fast, spin-polarized source of electrons taking advantage of the interband transitions might prove vital to studies of, e.g., quantum degenerate sources of electrons [40].

ACKNOWLEDGMENTS

We thank Dr. Maria Becker for her assistance with these experiments. This work was completed utilizing the Holland Computing Center of the University of Nebraska, which receives support from the University of Nebraska Office of Research and Economic Development, and the Nebraska Research Initiative. This work has been funded by NSF Grants No. PHY-2110358, No. 1806771, and No. 1505794 (T.J.G.); Grant No. EPS-1430519 (H.B. and T.J.G.), and No. NSF-2207697 (H.B.).

[1] D. T. Pierce and F. Meier, Photoemission of spin-polarized electrons from GaAs, Phys. Rev. B **13**, 5484 (1976).
[2] J. Kessler, *Polarized Electrons* (Springer, New York, 2013).
[3] P. Hommelhoff, Y. Sortais, A. Aghajani-Talesh, and M. A. Kasevich, Field emission tip as a nanometer source of free electron femtosecond pulses, Phys. Rev. Lett. **96**, 077401 (2006).
[4] B. Barwick, C. Corder, J. Strohaber, N. Chandler-Smith, C. Uiterwaal, and H. Batelaan, Laser-induced ultrafast electron emission from a field emission tip, New J. Phys. **9**, 142 (2007).
[5] E. Brunkow, E. R. Jones, H. Batelaan, and T. J. Gay, Femtosecond-laser-induced spin-polarized electron emission from a GaAs tip, Appl. Phys. Lett. **114**, 073502 (2019).
[6] W. Pfeiffer, F. Sattler, S. Vogler, G. Gerber, J.-Y. Grand, and R. Moller, Photoelectron emission in femtosecond laser assisted scanning tunneling microscopy, Appl. Phys. B **64**, 265(R) (1997).
[7] Y. Terada, S. Yoshida, O. Takeuchi, and H. Shigekawa, Laser-combined scanning tunnelling microscopy for probing ultrafast transient dynamics, J. Phys.: Condens. Matter **22**, 264008 (2010).
[8] J. R. Goldman and J. A. Prybyla, Ultrafast hot-electron dynamics in silicon, Semicond. Sci. Technol. **9**, 694 (1994); Ultrafast dynamics of laser-excited electron distributions in silicon, Phys. Rev. Lett. **72**, 1364 (1994).
[9] A. Othonos, Probing ultrafast carrier and phonon dynamics in semiconductors, J. Appl. Phys. **83**, 1789 (1998).
[10] A. Leitenstorfer, C. Fürst, A. Laubereau, W. Kaiser, G. Tränkle, and G. Weimann, Femtosecond carrier dynamics in GaAs far from equilibrium, Phys. Rev. Lett. **76**, 1545 (1996).
[11] D. J. Erskine, A. J. Taylor, and C. L. Tang, Dynamic Burstein-Moss shift in GaAs and GaAs/AlGaAs multiple quantum well structures, Appl. Phys. Lett. **45**, 1209 (1984).
[12] W. Z. Lin, L. G. Fujimoto, E. P. Ippen, and R. A. Logan, Femtosecond carrier dynamics in GaAs, Appl. Phys. Lett. **50**, 124 (1987).
[13] S. S. Prabhu and A. S. Vengurlekar, Dynamics of the pump-probe reflectivity spectra in GaAs and GaN, J. Appl. Phys. **95**, 7803 (2004).
[14] J. Shah, A. Pinczuk, A. C. Gossard, and W. Wiegmann, Energy-loss rates for hot electrons and holes in GaAs quantum wells, Phys. Rev. Lett. **54**, 2045 (1985).
[15] C. V. Shank, R. L. Fork, R. F. Leheny, and J. Shah, Dynamics of photoexcited GaAs band-edge absorption with subpicosecond resolution, Phys. Rev. Lett. **42**, 112 (1979).
[16] D. von der Linde and R. Lambrich, Direct measurement of hot-electron relaxation by picosecond spectroscopy, Phys. Rev. Lett. **42**, 1090 (1979).
[17] U. Hohenester, P. Supancic, P. Kocevar, X. Q. Zhou, W. Kütt, and H. Kurz, Subpicosecond thermalization and relaxation of highly photoexcited electrons and holes in intrinsic and p-type GaAs and InP, Phys. Rev. B **47**, 13233 (1993).
[18] P. Langot, N. Del Fatti, D. Christofilos, R. Tommasi, and F. Vallée, Femtosecond investigation of the hot-phonon effect in GaAs at room temperature, Phys. Rev. B **54**, 14487 (1996).
[19] N. Del Fatti, P. Langot, R. Tommasi, and F. Vallée, Temperature-dependent electron-lattice thermalization in GaAs, Phys. Rev. B **59**, 4576 (1999).
[20] F. Vallée and F. Bogani, Coherent time-resolved investigation of LO-phonon dynamics in GaAs, Phys. Rev. B **43**, 12049 (1991).
[21] P. Langot, R. Tommasi, and F. Vallée, Nonequilibrium hole relaxation dynamics in an intrinsic semiconductor, Phys. Rev. B **54**, 1775 (1996).
[22] C. S. Wang and B. M. Klein, First-principles electronic structure of Si, Ge, GaP, GaAs, ZnS, and ZnSe. I. Self-consistent energy bands, charge densities, and effective masses, Phys. Rev. B **24**, 3393 (1981).
[23] E. Brunkow, Investigations of novel sources of spin-polarized electrons, Ph.D. thesis, University of Nebraska-Lincoln 2018.
[24] S. Tiwari and S. L. Wright, Material properties of p-type GaAs at large dopings, Appl. Phys. Lett. **56**, 563 (1990).
[25] S. D. Benjamin, H. S. Loka, A. Othonos, and P. W. E. Smith, Ultrafast dynamics of nonlinear absorption in low-temperature-grown GaAs, Appl. Phys. Lett. **68**, 2544 (1996).
[26] X. Q. Zhou, H. M. van Driel, W. W. Rühle, and K. Ploog, Direct observation of a reduced cooling rate of hot carriers in the presence of nonequilibrium LO phonons in GaAs:As, Phys. Rev. B **46**, 16148 (1992).
[27] Y. A. Pusep, M. D. Teodoro, V. Laurindo, E. R. Cardozo de Oliveira, G. M. Gusev, and A. K. Bakarov, Diffusion of photoexcited holes in a viscous electron fluid, Phys. Rev. Lett. **128**, 136801 (2022).
[28] P. Lambropoulos and X. Tang, Multiple excitation and ionization of atoms by strong lasers, J. Opt. Soc. Am. B **4**, 821 (1987).

[29] T. Scarborough, Ultrafast intense-field photoionization and photofragmentation of systematic series of substituted organic molecules, Ph.D. thesis, University of Nebraska-Lincoln, 2012.

[30] J. R. Chelikowsky and M. L. Cohen, Nonlocal pseudopotential calculations for the electronic structure of eleven diamond and zinc-blende semiconductors, Phys. Rev. B **14**, 556 (1976).

[31] C. Kittel and P. McEuen, *Introduction to Solid State Physics* (Wiley, New York, 2018).

[32] R. N. Zitter, Saturated optical absorption through band filling in semiconductors, Appl. Phys. Lett. **14**, 73 (1969).

[33] T. Gong, W. L. Nighan, Jr., and P. M. Fauchet, Hot-carrier Coulomb effects in GaAs investigated by femtosecond spectroscopy around the band edge, Appl. Phys. Lett. **57**, 2713 (1990).

[34] J. S. Blakemore, Semiconducting and other major properties of gallium arsenide, J. Appl. Phys. **53**, R123 (1982).

[35] E. D. Palik, *Handbook of Optical Constants of Solids* (Academic, New York, 1998).

[36] L. Kronik and Y. Shapira, Surface photovoltage phenomena: Theory, experiment, and applications, Surf. Sci. Rep. **37**, 1 (1999).

[37] Q. Liu, C. Chen, and H. Ruda, Surface photovoltage in undoped semi-insulating GaAs, J. Appl. Phys. **74**, 7492 (1993).

[38] P. Siffalovic, M. Drescher, and U. Heinzmann, Femtosecond time-resolved core-level photoelectron spectroscopy tracking surface photovoltage transients on p–GaAs, Europhys. Lett. **60**, 924 (2002).

[39] S. Krishnamurthy, M. van Schilfgaarde, and N. Newman, Spin lifetimes of electrons injected into GaAs and GaN, Appl. Phys. Lett. **83**, 1761 (2003).

[40] M. Kuwahara, Y. Yoshida, W. Nagata, K. Nakakura, M. Furui, T. Ishida, K. Saitoh, T. Ujihara, and N. Tanaka, Intensity interference in a coherent spin-polarized electron beam, Phys. Rev. Lett. **126**, 125501 (2021); see also H. Batelaan, S. Keramati, and T. J. Gay, Comment on "intensity interference in a coherent spin-polarized electron beam," *ibid.* **127**, 229601 (2021).